Collateral RNA cleavage by CRISPR-Cas13 allows selective cell elimination

Cas13 collateral cleavage in eukaryotic cells

Jorik F. Bot[1,2 *], Zhihan Zhao[1,2 *], Darnell Kammeron[1,2], Peng Shang[1,2,‡] and Niels Geijsen[1,2,‡]

[1] Dept. of Anatomy & Embryology, Leiden University Medical Center, Einthovenweg 20, 2300 RC Leiden, The Netherlands.

[2] The Novo Nordisk Foundation Center for Stem Cell Medicine (reNEW), Leiden node, The Netherlands

* These authors contributed equally to this work.

‡ Leiden University Medical Center, Dept. of Anatomy & Embryology, Building 2, Einthovenweg 20, 2300 RC Leiden, The Netherlands. +31-(0)71-526 9302, n.geijsen@lumc.nl

Abstract

CRISPR-Cas13 systems are unique among Class II CRISPR systems, as they exclusively target RNA. *In vitro* and in prokaryotic cells, Cas13 cleaves both target and non-target RNA indiscriminately upon activation by a specific target RNA. This property has been exploited for development of diagnostic nucleic acid detection tools. In eukaryotic cells, CRISPR-Cas13 initially seemed to exclusively cleave the target RNA and consequently, CRISPR-Cas13 has been adopted as a specific RNA knockdown tool. Recently, several groups have reported unexpected toxicity or collateral cleavage when using CRISPR-Cas13 in eukaryotic cells, which seems difficult to reconcile with the reported target specificity. To understand these seemingly contradicting findings, we explored the collateral cleavage activity of six Cas13 systems, and show that only the most active ortholog *in vitro*, LbuCas13a, exhibits strong collateral RNA cleavage activity in human cells. LbuCas13a displayed collateral cleavage in all tested cell lines, targeting both exogenous and endogenous transcripts and using different RNP delivery methods. Using Nanopore sequencing, we found that cytoplasmic RNAs are cleaved without bias by LbuCas13a. Furthermore, the cleavage sites are highly specific and often present in Uracil containing single stranded RNA loops of stem-loop structures. In response to collateral RNA cleavage, cells upregulate stress and innate immune response genes and depending on target transcript levels, RNA degradation resulted in apoptotic cell death. We demonstrate that LbuCas13a can serve as a cell selection tool, killing cells in a target RNA specific manner. As such, CRISPR-Cas13 is a promising new technology that might be useful in anti-tumor applications.

Introduction

CRISPR-Cas is a prokaryotic adaptive immune system that protect bacteria and archaea from invading viruses and plasmids[1–3] . Since its initial discovery, an impressive diversity of CRISPR-Cas systems have been revealed[4]. Especially the Class 2 DNA targeting effector proteins, Cas9 and Cas12, have been extensively studied and have found widespread adoption for biotechnological and clinical use[5,6]. A recently discovered Class 2 system, CRISPR-Cas13, targets and cleaves RNA. The signature element of CRISPR-Cas13 systems are the two Higher Eukaryotes and Prokaryotes Nucleotide-binding (HEPN) RNase domains of the effector protein[7,8]. When a Cas13 protein is activated by a guide-matching target RNA, these domains cooperate to form a single active RNA nuclease site[9–15]. This catalytic site is located on the outside of the protein, facing away from the guide RNA-target RNA complex[16–20]. As a consequence, Cas13 cleaves both target and non-target RNA indiscriminately *in vitro*[9–13,15,21] and in bacteria[9,10,12,22] when activated by a specific target RNA. *In vitro,* this collateral RNA cleavage has been employed to develop portable, rapid, and highly sensitive nucleic acid detection methods[23–26], including for Coronavirus disease 2019 (COVID-19) diagnostics[27–29]. In bacteria, collateral RNA cleavage probably serves to protect bacterial communities by inducing dormancy after phage infection[22,30].

Unexpectedly, no evidence of collateral cleavage was found when Cas13 was first applied in eukaryotic cells[11,14,31]. Instead, Cas13 induced efficient and specific target RNA knockdown. Because Cas13-based knockdown was shown to have higher specificity and efficiency than RNAi[11,14,31–35] and CRISPRi[11,35], it has seen enthusiastic adoption as a specific RNA knockdown tool. For example, Cas13 has been adapted for use in mice[32,36–38], fish[36,39], yeast[40], fly[35], plants[41,42], and as an anti-viral[43–45] tool, with all groups reporting

seemingly specific RNA knockdown. However, there have been some conflicting reports which suggest that Cas13 is capable of collateral cleavage in eukaryotes in certain conditions[13,46–52], with one even encountering lethality in mice[50]. Given these contradicting findings, it is difficult to reconcile the collateral cleavage activity observed by some with the reported high specificity of Cas13-based knockdown in eukaryotes observed by others.

To understand these seemingly contradicting findings, we analyzed the activity of different Cas13 orthologs upon intracellular delivery of recombinant Cas13a protein and guide RNA in eukaryotic cells. We found that LbuCas13a displayed strong collateral cleavage, while the other orthologs displayed limited or no detectable collateral activity in eukaryotic cells, potentially explaining some of the seemingly conflicting reports by other groups. Next, we tested under which conditions LbuCas13a exhibited collateral cleavage. Collateral activity was found in all tested cell lines (including HEK293), using different RNP delivery methods, and using both endogenous or exogenous transcripts as targets. Using nanopore sequencing, we observed that upon mRNA-target dependent activation, LbuCas13a induces indiscriminate global mRNA cleavage. This cleavage occurs at very specific positions, often in the loops of stem-loop structures. With live cell imaging, we show that the collateral cleavage activity of LbuCas13a can trigger target-mRNA specific apoptosis and RNA-seq suggests that cells respond to widespread collateral RNA cleavage by inducing genes related to the innate immune response. Finally, we conducted a proof-of-concept experiments to demonstrate that LbuCas13a can be used as a cell selection tool to specifically eliminate cell types from a heterogenous cell population. We found that the cytotoxic effect of Cas13a strongly correlated with the expression level of the mRNA target. As such, LbuCas13a displays high collateral RNA cleavage activity inside human cells and can be used as

an effective cell selection tool, whereby specificity and efficacy are mediated by both mRNA target specificity as well as mRNA target expression levels.

Results

LbuCas13a exhibits collateral cleavage in human cells

The activity of different Cas13 orthologs *in vitro* is known to range over seven orders of magnitude[23]. We hypothesized that the Cas13 orthologs with the strongest collateral cleavage activity *in vitro* are the most likely to show any collateral cleavage in human cells. Therefore, we compared the collateral RNA cleavage activity of six different CRISPR-Cas13 systems (LbuCas13a, LwaCas13a, LshCas13a, BzCas13b, PspCas13b and RspCas13d) *in vitro* as well as in cells. We produced and purified all six recombinant proteins (Supplementary Figure 1A) and assessed their *in vitro* collateral RNA cleavage activity using the RNaseAlert® assay (Integrated DNA technologies), which quantitatively detects RNase activity (Figure 1A). We did not detect any collateral cleavage using LshCas13a, but the other orthologs displayed different levels of collateral RNA cleavage activity, which increased with increasing target RNA concentrations. Of these, LbuCas13a consistently demonstrated the strongest collateral cleavage activity, followed by RspCas13d. To test these orthologs in human cells, we transduced ribonucleoprotein (RNP) into cells using ‘induced transduction by osmocytosis and propanebetaine’ (iTOP), a previously reported method for the intracellular delivery of recombinant CRISPR-Cas RNPs[53]. Since LshCas13a did not have any detectable *in vitro* collateral activity, we did not include it in the cell-based experiments. We delivered the five remaining Cas13 proteins either with a non-targeting

or a dEGFP targeting guide RNA in HAP1 cells stably overexpressing a mutant, fluorescence-inactivated EGFP[54] (dEGFP^{Y66S}, referred to as dEGFP from hereon), and isolated RNA fifty minutes after RNP transduction. While RT-qPCR has been commonly used to assess for collateral RNA cleavage[55], this approach may not be suitable, as it depends on the assumption that the expression of a reference transcript is unaffected by the treatment. If Cas13 indeed behaves as a non-specific RNase, and also degrades the reference transcripts, this assumption no longer holds. Therefore, we decided to use a modified RT-qPCR strategy, which compares the relative quantity of the 3' part of a transcript to the 5' parts of the same transcript, thereby quantifying RNA integrity[56] (Figure 1B). In this assay, cDNA is created by reverse transcription using oligo dT primers, driving cDNA synthesis from the 3' end of the mRNA transcript. Thus, transcript cleavage by Cas13 results in a 3' bias. Consequently, a 5' located qPCR primer pair is expected to return higher Cq values than a 3' located qPCR primer pair. The difference in Cq values between the 3' and 5' primer pairs compared to controls is a reliable measure for the cleavage of that transcript. Indeed, targeting of dEGFP using LbuCas13a, LwaCas13a, PspCas13b and BzCas13b, resulted in an increase in 5' Cq values relative to 3' for the dEGPF transcript, indicating that these orthologs efficiently cleaved the target RNA in HAP1 cells (Figure 1C). Surprisingly, RspCas13d did not show significant target RNA cleavage. Only dEGFP targeting with LbuCas13a resulted in significant degradation of GAPDH mRNA, indicating collateral RNA cleavage inside the treated cells. LwaCas13a, BzCas13b and PspCas13b showed a minimal increase in 5' Cq values, suggesting low levels of collateral cleavage, but these were not significant over the non-targeting control. Taken together, we observed that although five out of six Cas13 orthologs tested exhibited collateral cleavage activity *in vitro*, only LbuCas13a demonstrated significant collateral and on-target RNA cleavage activity in human cells.

Temporal dynamics of target and collateral RNA cleavage

Next, we investigated the temporal dynamics of the in-cell target and collateral RNA cleavage after RNP transduction. We transduced LbuCas13a protein and a dEGFP-targeting guide RNA into either wild-type or dEGFP-expressing cells and collected total RNA at various timepoints after transduction. The total RNA integrity was then analyzed using the 2100 Bioanalyzer (Agilent). While the total RNA of wildtype cells was intact at all timepoints, the total RNA profile of dEGFP expressing cells clearly revealed a degradation pattern mainly consisting of several novel fragments preceding the 18S rRNA peak. Due to their relative abundance and specific size, we speculate that these fragments are rRNA cleavage products (Figure 1D). Collateral (rRNA) cleavage was time dependent and peaked at 100-200 minutes after Cas13a transduction, with some cleavage fragments remaining at 24 hours post transduction. Using the 3':5' RT-qPCR assay, we observed both target RNA (dEGFP) and collateral RNA (GAPDH) cleavage (Figure 1E). While target cleavage seemingly started almost immediately, GAPDH cleavage started later and peaked at around 100 minutes after Cas13a transduction. Both target and collateral (GAPDH) RNA integrity returned to normal from about 500 minutes post transduction. Finally, we noticed that the total amount of RNA isolated per well was greatly decreased in the dEGFP expressing cells at 24 hours post transduction, which is likely a consequence of both the collateral RNA cleavage and cell loss due to toxicity of collateral RNA cleavage (Supplementary Figure 1B).

Exploring the requirements for Cas13 collateral cleavage in human cells

Since previous reports demonstrated that Cas13 does not display collateral cleavage in certain cell lines[55], we explored whether collateral RNA cleavage was perhaps cell-type dependent. In addition, we examined if LbuCas13a collateral cleavage could also be induced targeting

endogenous transcripts and using a different RNP delivery method. First, we transduced the chronic myeloid leukemia derived line HAP1, the rhabdomyosarcoma line RD, the osteosarcoma line U2OS, and the retinal pigment epithelia line ARPE19 with LbuCas13a and guides targeting the highly abundant endogenous transcripts RPS19, GAPDH, or 18S rRNA. All four cell lines demonstrated robust collateral cleavage after targeting any of these target transcripts (Figure 2A-F). Notably, the degradation pattern was exactly the same in all conditions, suggesting that the collateral cleavage sites do not depend on the target RNA or cell line. This consistent RNA degradation pattern allowed us to quantify the total RNA degradation by taking the area under the curve of the region where most of the cleaved RNA fragments occur (See Figure 2A). Across all four cell lines, 18S rRNA targeting resulted in the most robust collateral RNA cleavage activity, followed by GAPDH and RPS19 respectively (Figure 2B). We hypothesize that targeting 18S rRNA was the most effective due to the high abundance of this transcript. HAP1 cells consistently demonstrated more total RNA degradation than the other three cell lines, suggesting that the cellular environment, efficiency of iTOP delivery or the particularly small cell size of these cells positively influence LbuCas13a activity. We utilized the 3':5' RT-qPCR method to further quantify the collateral cleavage effect in these samples. RNA degradation was presented by both an overall increase in Cq values compared to untreated cells as well as an increased difference between the 5' and 3' primer pair (Figure 2G). However, trends differed between cell lines. For HAP1 and RD the difference between the 5' and 3' primer pair was prominent, with HAP1 also showing a big overall increase in Cq values. But for U2OS and ARPE19 the main effect seemed to be an overall increase in Cq values for both primer pairs, displaying more modest differences between the 5' and 3' primers.

To exclude that the transduction method somehow facilitates collateral cleavage, we examined the effect of LbuCas13 protein and guide RNA delivery by electroporation. Electroporation also resulted in strong rRNA degradation when targeting RPS19, GAPDH or 18S rRNA in HAP1 cells, demonstrating that collateral cleavage is not the result of our iTOP delivery method (Supplementary figure 2A).

Several reports showing specific RNA knockdown with Cas13 used HEK293T cells[11,14,31], while others explicitly report low or even the absence of collateral cleavage in this cell type[46,52], suggesting that Cas13 may be less active in HEK293T cells. Using electroporation to deliver LbuCas13a protein and guide RNA in HEK293T cells, we observed the characteristic RNA degradation pattern upon targeting GAPDH and 18S rRNA (Supplemental figure 2B), indicating that HEK293T cells are not intrinsically protected against collateral cleavage activity. However, in agreement with above mentioned publications, upon targeting 18S rRNA, the extent of the collateral cleavage was decreased compared to HAP1 and nearly absent when targeting GAPDH and RPS19 respectively.

From above experiments, we conclude that collateral cleavage peaks at around 100 minutes post transduction, yet we initially compared the different Cas13 orthologs at only 50 minutes post transduction. Furthermore, targeting 18S rRNA, a highly abundant RNA in all cells, results in the highest collateral cleavage activity in all tested cell types. We wondered whether we could also detect a specific total RNA degradation pattern for the other Cas13 orthologs using these optimized conditions. Therefore, we re-tested LwaCas13a, BzCas13b and RspCas13d, this time isolating total RNA after 100 minutes and targeting either GAPDH, dEGFP or 18S rRNA in HAP1 cells. Targeting GAPDH or dEGFP with LwaCas13a did not change the total RNA profile, however 18S rRNA cleavage resulted in two additional peaks smaller in size than the 18S rRNA

(Supplementary Figure 3A). As 18S rRNA was the target RNA, this probably represents target RNA cleavage. Using BzCas13b resulted in a small extra peak between the 18S and 28S rRNA peak when targeting dEGFP or 18S rRNA (Supplementary Figure 3B). Furthermore, RNAs smaller than 5S RNA and tRNA increased in abundance, which possibly represents the emergence of cleavage products of BzCas13b activity. None of the samples using RspCas13d showed any alteration to the total RNA profile, suggesting that RspCas13d does not work well in human cells (Supplementary Figure 3C).

In conclusion, LbuCas13a is capable of collateral cleavage in all tested cell lines, independent of RNP delivery method, and targeting both exogenous and endogenous transcripts. Given that LbuCas13a consistently showed the strongest collateral cleavage *in vitro* and in cells, we decided to use LbuCas13a for all further experiments characterizing the mechanism and cellular consequences of collateral cleavage in human cells.

Characterizing collateral RNA cleavage using nanopore sequencing

To further explore the identity of the RNAs that are subject to collateral cleavage, as well as the dynamics of the collateral cleavage process, we performed Nanopore sequencing. HAP1 cells were transduced with LbuCas13a and either a non-targeting or a dEGFP targeting guide RNA. Total RNA was collected at 0, 50, 200, 500 and 1440 minutes after transduction. Collateral cleavage activity was apparent in the total RNA profiles (Supplementary Figure 4A). We used rRNA depletion to remove rRNA (Supplementary Figure 4B). In order to also detect cleaved RNA fragments without a poly-A tail in the nanopore sequencer, we included a polyadenylation step before reverse transcription with anchored oligo(dT) primers. Next, second strand

synthesis was performed using random primers. Finally, barcodes and nanopore adopters were ligated, and samples were sequenced on the PromethION sequencing platform. Read lengths of dEGFP targeting samples were much shorter than control samples (Supplementary figure 4C), containing markedly fewer reads bigger than 1000 nt, demonstrating widespread LbuCas13a-mediated collateral RNA cleavage. Next, reads were mapped to the combined Ensemble cDNA and ncRNA transcriptomes using minimap2[57]. We found that when targeting dEGFP, the amount of protein coding transcripts decreased relative to all other transcripts biotypes (Supplementary Figure 5A). On the other hand, the percentage of reads mapping to lncRNAs, snoRNAs, and (in replicate 1) snRNAs increased, suggesting that nuclear RNAs were relatively protected from collateral cleavage. This is expected, because the LbuCas13a protein we used does not contain a nuclear localization signal.

The abundance and read length of reads mapped to protein coding transcripts greatly decreased at 50 and 200 minutes post transduction (Figure 3A and Supplementary Figure 5B). At these timepoints, almost all reads were (much) shorter than the reference they mapped to, whereas most reads in the empty transduction and non-targeting controls were full length transcripts. This suggests unbiased cleavage of all mRNAs after LbuCas13a activation by dEGFP.

Next we explored the dynamics of cleavage of individual transcripts by calculating their relative transcript coverage. A coverage value of 1 means that 100% of the reads mapped to the transcript cover that specific nucleotide position. If a transcript has been subjected to cleavage, reads of cleavage products will only cover part of the transcript, thus decreasing the relative overall coverage. In the mock transduction and non-targeting control samples, we observed that short transcripts like RPS19-202, GAPDH-205 and ACTB-217 had stable and high read

coverage across the entire transcript (Figure 3C, Supplementary Figures 7B and 7C). Longer transcripts, like dEGFP-IRIS-PuroR and PKM-202, showed a gradual increase in coverage from the 5' to 3' side (Figure 3B, Supplementary Figure 7A). This may be caused by higher susceptibility to breakage of longer transcripts, incomplete reverse transcription, the use of random primers for second strand synthesis, or incomplete sequencing events. Finally, coverage analysis revealed that the RNA quality of the 0, 50 and 200 minute samples of replicate 2 was somewhat lower than replicate 1. Nevertheless, the transcript coverage in the targeting samples clearly decreased compared to the control conditions for all these transcripts. At 50, 200 and 500 minutes post transduction, the overall coverage of dEGFP-IRIS-PuroR is much lower for the dEGFP targeting samples than the empty transduction and non-targeting control conditions (Figure 3B). Additionally, the target RNA shows a decrease in coverage at the exact location of the protospacer at all timepoints (Figure 3B, dotted lines), which fits with the 3':5' qPCR data that showed target RNA cleavage immediately after transduction (Figure 1E). This suggest LbuCas13a cleaves in, or very near the protospacer, which is surprising since others have shown that Cas13 cleavage sites do not depend on protospacer position[9–11]. Alternatively, the protospacer specific dip in coverage may be a technical artifact, for example, due to LbuCas13a still being bound to the target RNA after purification, preventing complete reverse transcription of this location. In addition to the coverage dip around the protospacer, additional dips in coverage were observed, which are consistent between timepoints and replicates. We suspect that these are LbuCas13a cleavage sites. Non-target (collateral) mRNAs, like RPS19-202, GAPDH-205, ACTB-217 and PKM-202 also show these consistent dips in coverage at 50, 200 and (to a lesser extend) 500 minutes after transduction in very specific positions, indicating collateral cleavage of these transcripts (Figure 3C, Supplementary

Figures 6). Besides mRNAs, cytoplasmic ncRNAs (RN7SL1, 18S rRNA and 28S rRNA) also seems to be cleaved by LbuCas13a (Supplementary Figure 7). The 18S rRNA has one unique dip in transcript coverage around position 780 in the targeting samples (Supplementary Figure 7B), suggesting a single cleavage site. On the other hand, 28S rRNA seems to be cleaved at multiple locations (Supplementary Figure 7C). We do not observe any differences in coverage between targeting and control samples for small nuclear or mitochondrial RNAs (Supplementary Figure 8), again suggesting that our LbuCas13a protein mostly acted in the cytoplasm. However, fragments smaller than 100 nt are not expected to survive library preparation. Since most nuclear RNAs are between 100 and 200 nt long, their cleavage fragments may therefore have been lost during library preparation.

The dips in transcript coverage tend to be 10-20 nucleotides wide, so we cannot discern the exact cleavage position (Figure 4A). *In vitro*, LbuCas13a was shown to prefer cleaving at uracil residues in or near single stranded loop structures[23]. Indeed, in our data, transcript coverage dips often map to predicted stem-loop structures, with uracil containing single stranded loops on the 5’ side of the coverage dip (Figure 4B), suggesting that the 5’ side of the coverage dip is the actual cleavage location. This suggests that LbuCas13a cleavage preferences follow the same pattern in human cells as observed *in vitro*. Next, we manually annotated 100 potential cleavage sites (supplementary table 4), assuming that the Uracil closest to the 5’ side of the coverage dip was the cleavage position. These sites suggest a US (S = G or C) di-nucleotide preference (Figure 4C).

Taken together, the Nanopore sequencing provides further evidence of collateral cleavage in human cells by LbuCas13a and reveals that both mRNAs and cytoplasmic ncRNAs are cleaved

without bias. Additionally, it shows that LbuCas13a prefers to cleave RNA at specific positions and our data suggests a preference for uracil-containing single stranded loop structures.

Cellular response to collateral RNA cleavage by LbuCas13a

Over the course of our experiments, we noticed that cells were rounding up and detaching from the bottom of the plate the day after target dEGFP with LbuCas13a (Figure 5A), suggesting cytotoxicity of the LbuCas13a collateral cleavage. To examine this further, we performed live cell imaging with Annexin V as a marker for early apoptosis and CellTox Green to stain for dead cells (targeting a non-fluorescent EGFP allows us to use this green dye)[58]. When cells die by necrosis they become positive for both these dyes simultaneously, however if they go into apoptosis, Annexin V staining precedes CellTox green staining. We tested three different guide RNAs targeting dEGFP, and transduced these into either wildtype or dEGFP expressing cells. When targeting dEGFP in wildtype cells, the amount of Annexin V and CellTox green positive cells was roughly similar to the empty transduction control (Figure 5B). However, for all three dEGFP targeting guide RNAs the number of Annexin V positive cells rapidly increased in dEGFP expressing cells approximately 7.5 hours after transduction, followed by an increase in CellTox Green positive cells approximately 15 hours after transduction (Figure 5B and Supplementary movies 1 and 2). This suggests that the cells die by apoptosis, not necrosis, which is consistent with results for other RNases, such as α-sarcin[59]. Furthermore, it shows that LbuCas13a-induced apoptosis is critically dependent on target RNA expression.

To gain further insight into the cellular response to the collateral RNA cleavage, we performed RNA sequencing 16 hours after transduction. We estimated that this timepoint was far enough removed from the peak in collateral RNA degradation to allow for RNA sequencing to be successful. Indeed, quality control by FastQC[60] and RSeQC[61] did not reveal any major issues. STAR[62] aligned sequences at similar rates across all conditions, however, a higher percentage of the reads from the dEGFP targeting samples mapped to introns compared to the controls, consistent with a relative increase in immature nuclear transcripts generated as a result of the global cytoplasmic RNA depletion in the cell (Supplementary Figure 9A).

For further analysis, we used the count table generated using featureCounts[63] after STAR alignment[62]. First, we performed principal component analysis (PCA) (Supplementary Figures 9B). The PCA plot shows a clear separation between the dEGFP targeting samples and the controls, suggesting that collateral cleavage by LbuCas13a leads to substantial changes in the transcriptome. Indeed, we found 721 significantly upregulated and 36 significantly downregulated genes (adjusted P-value < 0.05, $|\text{Log2 FC}| > 1$) in response to LbuCas13a activation (Figure 5C).

The relatively low number of downregulated genes and high number of upregulated genes is perhaps somewhat counterintuitive in the context of collateral cleavage, but consistent with another report documenting the cellular response to Cas13 collateral cleavage[50]. In agreement with Li et al., we observed that many of the upregulated genes we find are immediate early response genes, such as JUN, FOS, EGR1, EGR2, EGR3, EGR4 and ARC. Li and colleagues propose that translation impairment though loss of ribosomal RNA may be the underlying cause of the cellular stress response. However, blocking translation alone, for example using cycloheximide, usually does not results in apoptosis[59], and thus translation

impaired alone is probably not the sole cause of the LbuCas13-induced apoptosis. GO enrichment analysis of the significantly upregulated genes revealed an enrichment of many biological processes related to the innate cellular immune response (Figure 5D), with upregulation of transcripts related to chemokine and cytokine activity (Supplementary Figure 9C). Interestingly, we also observed in increase in genes involved in transcriptional activity, possibly an attempt to replace lost mRNAs due to collateral cleavage and consistent with our observed increase in nascent, intron-containing RNAs. KEGG pathway analysis also showed enrichment for immune related pathways, such as viral protein interaction with cytokine and cytokine receptor, IL17 signaling pathway, TNF signaling pathway and NF-kappa B signaling pathway (Supplementary Figure 9D). These are known factors of the cellular immune response that are triggered, for example, by intracellular recognition of viral RNA and suggests that the LbuCas13a-mediated collateral RNA cleavage and subsequent increase in 5’ uncapped RNA and 3’ ends without poly-A tail triggers a similar immune response which ultimately leads to apoptosis.

Application of LbuCas13a as an efficient cell selection tool

Given that target-activated collateral RNA cleavage by LbuCas13a induced cell death (Figure 5B), we wondered whether we could exploit this property to specifically eliminate cells that express the target RNA from a heterogeneous cell population (Figure 6A). To test this, we mixed fluorescent EGFP expressing HAP1 cells with WT HAP1 cells and transduced this mixed population with LbuCas13a and a guide RNA targeting EGFP. We then measured the percentage of EGFP positive cells by FACS over time. The percentage EGFP positive cells rapidly decreased when targeting EGFP (Figure 6B) with 36.3% EGFP-positive cells remaining

at day 6, compared to more than 60% EGFP positive cells when using a non-targeting guide (Figure 4B). Next we examined whether multiple sequential selection events could further eliminate the EGFP positive cell population (Figure 6C). We performed several serial transductions at 2 day intervals, with up to 3 subsequent selection rounds. Every additional selection round decreased the amount of EGFP positive cells in the population by approximately 20%. From the above data we conclude that Cas13-based cell-selection is target specific, repeatable and that multiple selection rounds can further improve the enrichment.

Target RNA expression level theoretically limits the number of active LbuCas13a molecules and therefore the amount of collateral cleavage, which could influence the efficiency of cell selection. To test this, we FACS sorted a heterogeneous population of EGFP expressing cells into cell populations with different levels of EGFP intensity (Figure 6D and Supplementary Figure 10A). RT-qPCR confirmed EGFP expression levels increased with EGFP intensity (Supplementary Figure 10B). We then tested the depletion efficiency of these cells with different EGFP expression levels by mixing them with WT HAP1 cells and targeting EGFP with LbuCas13a. In parallel we also performed RT-qPCR on these cell lines to quantify their EGFP expression at the time of the experiment. We found a strong correlation between the expression level of the target RNA and the depletion of EGFP positive cells (Figure 6E), suggesting that high levels of LbuCas13a activation result in more robust collateral RNA cleavage and a high probability of inducing cell death. Depletion efficiency seems to plateau at the highest levels of target RNA expression. At this point the RNP delivery efficiency may have become the limiting factor.

We next examined whether the same strategy could be used to positively select for cells that underwent successful gene editing. For these experiments we used a HAP1-EGFP$^{\Delta fluor}$ cell line

containing a 9 nt deletion in EGFP, rendering it non-fluorescent (Supplementary Figure 10C)[54]. Using this system, we previously reported Cas12a-mediated correction of EGFP fluorescence, with an efficiency of about 5%[54]. When we employed LbuCas13a and a guide RNA that targets the unedited cells as a cell selection tool, the percentage of EGFP expressing cells increased to around 15% (Figure 6F). Thus, a single round of selection using LbuCas13a resulted in a 3-fold enrichment. Altogether, these proof-of-principle studies show the potential of Cas13 as a potent cell selection tool, including the enrichment of successfully edited cells.

Discussion

In this study, we explored the behavior of the Class 2, type VI CRISPR-Cas13 systems in human cells. A peculiarity of CRISPR-Cas13 is that it cleaves both target and non-target RNA when activated. This non-target or collateral RNA cleavage is well established *in vitro*[9–13,15,21] and in bacteria[9,10,12,22], but initial reports could not find evidence of collateral RNA cleavage in eukaryotes, instead showing efficient and specific target RNA knockdown[11,14,31]. Consequently CRISPR-Cas13 has mainly seen development as a specific RNA knockdown tool, with reported specificities often greatly exceeding those of shRNAs[11,14,31–35]. Others, however, have run into unexpected toxicity and/or apparent collateral RNA cleavage when trying to use CRISPR-Cas13 in eukaryotic cells[46,48–52,64]. These conflicting observations are difficult to reconcile. From ours and others experiments, three factors are likely important in determining if and how much collateral cleavage occurs. First, collateral cleavage in human cells seems to require a highly active Cas13 ortholog. In this work, only LbuCas13a, which had

the highest *in vitro* collateral cleavage activity, exhibited readily detectable collateral cleavage in human cells when delivered as RNP. In addition, Tong et al. have shown that decreasing the activity of Cas13 mainly reduced collateral activity[65]. A reduction in activity will not necessarily result in a dramatic decrease in target RNA cleavage activity, because Cas13's guide RNA needs to base pair with the target RNA to activate Cas13. Cas13 is therefore in close proximity to the target RNA and is thus likely to cleave it. In contrast, collateral cleavage activity will decrease proportionally with decreased Cas13 activity. While other reports have documented collateral cleavage or toxicity using LwaCas13a[46,48], this ortholog is not sufficiently active in our hands. This could be a result of differences in cell line, target RNA or delivery strategy.

Second, in addition to Cas13 activity itself, we found that the levels of target RNA expression was also an important determinant of the extent of collateral cleavage activity. Other reports of collateral cleavage or toxicity by Cas13 have also observed that these effects are target RNA expression level dependent[51,52]. Even in bacteria, there seems to be an expression threshold which must be reached to induce dormancy or cell death[66]. This suggests that a single target RNA activates only one or at most a few Cas13 proteins, probably due to prolonged guide RNA-target RNA base pairing after activation.

Finally, target cell type appears to influence collateral cleavage activity, which is in agreement with other reports[51,52]. In addition to differences in Cas13 protein activity in different cell types, these cell line specific differences may also be caused by other factors such as delivery efficiency, promoter activity (when using expression systems) or Cas13 protein and guide RNA half-life. Several publications claiming collateral cleavage activity of Cas13 in eukaryotes do not detect any, or much lower collateral cleavage in HEK293T cells[46,48,50,52]. While we observed some collateral activity in HEK293T, overall collateral cleavage activity was reduced

compared to HAP1 cells. This suggests that although Cas13 seems capable of collateral cleavage in HEK293T, the particular cellular microenvironment somehow blunts it's activity.

In conclusion, the need for both a highly active Cas13 ortholog and high target RNA expression could explain why collateral activity does not always seem to occur. We recently proposed that the substantial difference in relative cell size between eukaryotes and bacteria might explain the need for both high activity and high target RNA expression[55]. In addition, since early Cas13 studies are based on HEK293T cells[11,14,31], which seem unusually resistant to Cas13, this might provide a- further explanation for why collateral cleavage was initially overlooked.

We noted that commonly used collateral cleavage detection methods, namely RT-qPCR and RNA-seq, are not suitable for the detection and quantification of collateral cleavage, because they are relative quantification methods. RT-qPCR relies on the stable expression of an intrinsic reference RNA[55]. In the case of Cas13-mediated collateral cleavage such reference RNA is itself subject to degradation. Here we showed that the 3':5' RT-qPCR assay may be a viable alternative to conventional RT-qPCR for assessing collateral RNA cleavage. Our predicted cleavage sites from the nanopore sequencing may provide a useful guide for where to design the 5' and 3' primer pairs, when using LbuCas13a. Furthermore, other reports suggest that exogenous RNA is cleaved more readily than endogenous RNA[13,50–52], making them preferred (3':5') RT-qPCR targets for collateral cleavage detection. Like RT-qPCR, RNA-seq is also a relative quantification method, and therefore not suitable for detecting an unbiased RNase. Indeed Shi *et al.* recently showed with spike in RNAs that collateral cleavage by RfxCas13d resulted in an almost uniform reduction in transcript abundance, which would

probably not lead to differential gene expression using conventional RNA-seq[51]. In this study, we used long read sequencing to explore collateral RNA cleavage. This allowed us to measure both the size of RNA fragments, and determine the location of the 5’ and 3’ ends. Nanopore sequencing suggested unbiased cleavage of cytoplasmic RNAs, in agreement with Shi and colleagues[51]. In addition, we showed that LbuCas13a preferred cleavage sites are similar to known *in vitro* preferences of LbuCas13a[21]. However, the relatively low number of reads received after nanopore sequencing only allowed us to predict cleavage sites of highly expressed genes. For truly transcriptome wide cleavage site prediction, utilizing 5’ and/or 3’ end sequencing protocols may be necessary. Taken together, the use of inadequate methods for collateral cleavage detection provides an additional explanation as to why many groups only detected target RNA cleavage.

In conclusion, this and other recent reports strongly suggest that CRISPR-Cas13 does not inherently behave differently in eukaryotic cells. This calls into question the utility of CRISPR-Cas13 as a specific RNA knockdown tool, especially targeting highly abundant transcripts. Collateral cleavage in eukaryotic cells by Cas13 does however create new opportunities. We demonstrated that LbuCas13a can be applied as an efficient and target RNA-specific cell selection tool. How collateral RNA cleavage induces cell death is still unclear, with our data suggesting the involvement of an innate immune response. Exploring this may improve future Cas13-based negative cell selection systems. Finally, Cas13-based negative cell selection may be used as cancer treatment, targeting unique oncogenic transcripts and thus only activating Cas13 in cancer cells.

Materials and Methods

Contact for reagent and resource sharing

Recombinant LbuCas13a and AsCas12a proteins, the HAP1-dEGFP^{Y66S} and the HAP1-dEGFP$^{\Delta fluor}$ cell lines are available through Divvly (https://divvly.com/geijsenlab).

Expression and purification of recombinant Cas13 proteins

All Cas13 orthologs were cloned into a pET15b expression vector (Addgene #62731). LbuCas13a and LshCas13a were a gift from Jennifer Doudna (Addgene plasmids #83482 and #83487). LwaCas13a, BzCas13b and PspCas13b were a gift from Feng Zhang (Addgene plasmids #91924, #89898 and #103862). RspCas13d was a gift from Arbor Biotechnologies (Addgene plasmid #108304). The sequence of the expression vectors is available in supplementary file 1. Expression vectors will be made available on Addgene. The different Cas13 orthologs were expressed and purified as described previously for Cas12[54]. The purified Cas13 protein was concentrated to 75 µM using the Amicon ultra centrifugal filter, MWCO 50 kDa (Merck).

Preparation of guide RNAs and target RNA by *in vitro* transcription

Oligonucleotides carrying the T7 promoter and appropriate downstream sequence were synthesized by IDT and PCR-amplified to generate *in vitro* transcription (IVT) templates (see supplementary table 1 for template and primer sequences). The EF-1a_dEGFP^{Y66S}-IRIS-PuroR-WPRE plasmid (supplementary file 1) was used as PCR template to generate the IVT template for the target RNA. Transcription reactions were performed at 37°C for 4 hours in a buffer

containing 40 mM Tris-HCl (pH 8), 20 mM $MgCl_2$, 5 mM DTT, 2 mM NTPs, 50 µg/mL T7 RNA polymerase, and 250 ng/µL DNA template. Next, to remove the DNA template, 1 µL Turbo DNase (Invitrogen: AM2238) per 100 µL IVT reaction was added and incubated at 37ºC for 30 minutes. The RNA was then purified using the Zymo RNA Clean & Concentrator -25 kit (R1017). Typically, four different guide RNAs were tested for each target RNA, assessing collateral cleavage by comparing total RNA degradation using the Bioanalyzer (see below). The guide RNA with the highest amount of total RNA degradation was selected for use in experiments.

In vitro collateral cleavage activity assay

Collateral RNA cleavage detection assays were performed with IDT RNaseAlert (IDT, 11-04-02-03) according to the manufacturer's protocol. Reactions were performed in different cleavage buffers depending on the Cas13 ortholog. For LshCas13a, LwaCas13a and LbuCas13a the buffer[9] consisted of 40 mM Tris-HCl pH 7.3, 60 mM NaCl and 6 mM $MgCl_2$. For Cas13b (BzCas13b and PspCas13b), the cleavage buffer contained 10 mM Tris-HCl pH 7.5, 50 mM NaCl and 0.5 mM $MgCl_2$[10]. For RspCas13d, the cleavage buffer used was 20 mM HEPES pH 7.1, 50 mM KCl, 5 mM $MgCl_2$ and 5% glycerol[12]. Before the RNaseAlert assay, 1 µM Cas13 and 500 nM guide RNA were preassembled in 10X cleavage buffer for 10 min at 37°C. The RNaseAlert assays were performed using 100 nM Cas13 protein and 50 nM guide RNA with the appropriate amount of target RNA, using a 50 µL reaction volume. Reactions were prepared on ice, in opaque 96-well plates (Greiner, 655076). Fluorescence was measured every 5 minutes using a Tecan Spark plate reader, while incubating at 37ºC. Reactions were allowed to proceed

for at least one hour. The collateral cleavage rate was calculated in Excel by applying the SLOPE function to the initial linear increase in fluorescence.

Cell culture

HAP1 cells were a gift from Dr. Brummelkamp, NKI Amsterdam. RD cells were a gift from Dr. Gerben Schaaf, Erasmus MC. HEK293T cells were ordered from Takara (#632180). U2OS and ARPE19 cells were ordered from ATCC (HTB-96 and CRL-2302 respectively). All cell lines were tested for mycoplasma monthly.

HAP1 cells were cultured in Iscove's Modified Dulbecco's Medium (IMDM) supplemented with 10% Fetal Bovine Serum (FBS). HEK293T cells were cultured in Dulbecco's Modified Eagle Medium (DMEM) with 10% FBS. U2OS and RD cells were cultured in DMEM supplemented with 10% FBS and 2mM L-Glutamine. ARPE19 cells were cultured in DMEM/F12 with 10% FBS. All culture medium was purchased from Gibco. All cells were grown at 37°C in a humidified atmosphere containing 5% CO_2.

To generate the HAP1-dEGFP^{Y66S}, HAP1-dEGPF$^{\triangle fluor}$ and HAP1-EGPF lines, HAP1 cells were transfected with the EF-1a_dEGFP^{Y66S}-IRIS-PuroR-WPRE, EF-1a_EGFP$^{\triangle fluor}$-IRIS-PuroR-WPRE or EF-1a_EGFP-IRIS-PuroR-WPRE plasmids (supplementary file 1) using lentivirus (previously made in Geijsenlab, unpublished). Two days after transfection, puromycin selection was started at 0.5 µg/mL to select for integration of the plasmid. After resistant cells had established themselves, the puromycin concentration was increased every 2 days to 1, 2, 5 and

finally 10 µg/mL. HAP1-dEGFP^{Y66S}, HAP1-dEGFP$^{\triangle fluor}$ and HAP1-EGFP cells were maintained in HAP1 medium supplemented with 10 µg/mL puromycin.

Ribonucleoprotein transduction using iTOP

The Cas13 proteins and their guide RNAs were transduced into target cells using iTOP, using a protocol adapted from D'Astolfo et al.[53]. The iTOP protocol consists of four steps: (1) seeding the cells, (2) iTOP transduction mixture preparation, (3) incubating the cells in the iTOP mixture, and (4) recovery. First, cells were plated the day before transduction in Matrigel coated pates (Corning: 356231, diluted 1:100 in PBS), such that the confluency was ~70% the next day. Second, to prepare the iTOP transduction mixture, 2/5 of transduction supplement B (Opti-MEM media supplemented with 810 mM NaCl, 504 mM GABA, 1.875X concentrated N2 (Gibco: 17502048), 1.875X concentrated B27 (Gibco: 17504044), 1.875X concentrated MEM non-essential amino acids (Gibco: 11140050), 3.75 mM L-Glutamine (Gibco: 25030081), 2.5 µg/mL bFGF (Gibco: PHG0023), and 0.625 µg/mL EGF (Gibco: PHG0313)), 1/5 of Cas13 protein (75 µM) or empty protein storage buffer (see Zhao et al.[54]), 1/5 of guide RNA (75 µM) or nuclease-free water, and finally 1/5 nuclease-free water were combined. iTOP mixture volumes used per well were: 50 µL for 96-well plates, 150 µL for 48-well plates, 200 µL for µ-slide 8-well (ibidi, 80827) and 1000 µL for 6-well plates. Third, the culture medium was aspirated and iTOP mixture was carefully added into the wells. Next the cells were returned to the cell culture incubator for 45 minutes. Fourth, immediately after incubation the iTOP mixture was aspirated and replaced by pre-warmed cell culture medium (96-well: 200 µL, 48-well: 600 µL, µ-slide 8-well: 300 µL, 6-well: 4000 µL. Finally cells were returned to the cell culture incubator or immediately harvested for downstream analysis.

Ribonucleoprotein transduction using electroporation

A Lonza Nucleofector system including a Nucleofector 2b Device and the Cell Line Nucleofector Kit V (Lonza) were used for electroporation of LbuCas13a protein and guide RNA, according to the manufactures instructions. One million cells were used per electroporation, resuspended in 100 µL Nucleofector solution V buffer containing 1 µM LbuCas13a and 1 µM guide RNA. The electroporation was performed in the Nucleofector 2b device using the ‘Cell-line T-020’ program. After electroporation, the cells were incubated at 37°C and the culture medium was changed after 16 hours.

Total RNA isolation

Cells were collected in TRIzol reagent (Invitrogen: 15596018) and stored at -80°C until RNA isolation. To isolate total RNA, 0.2 mL of chloroform per 1 mL of TRIzol was added and samples were mixed by briefly vortexing. Next, samples were centrifuged for fifteen minutes at twelve thousand x g at 4°C. Total RNA was isolated from the colorless upper aqueous phase using the Zymo RNA Clean & Concentrator -5 kit, including an in-column DNase treatment, according to the manufacturer’s instructions.

Bioanalyzer

Total RNA integrity was analyzed on the Bioanalyzer using either the RNA nano or RNA pico chips, depending on the available RNA amount. The area under the curve (AUC) was calculated in R with the “AUC” function from the DescTools package using the default settings[67]. To

account for differences in the amount of RNA loaded, all samples were normalized to their total AUC. This was done by dividing the sample fluorescence by the sample AUC and multiplying by the mean AUC across all samples. In our hands, this method resulted in a more accurate normalization than using the sample concentration estimates supplied by the Bioanalyzer software.

3':5' RT-qPCR

RNP transduction by iTOP was performed in 96-well plates, as described above. Besides LbuCas13a and either a targeting or a non-targeting guide RNA, an empty transduction control was always included. All 3':5' ddCq values are relative to this empty transduction control. Total RNA was isolated and DNase-treated as described above. An anchored oligo(dT) primer was used for reverse transcription using SuperScript III reverse transcriptase (Invitrogen, 18080093), according to the manufacturer's protocol. qPCR was performed in triplicate using Bio-Rad iQ SYBR Green Supermix with 300 nM primers. The primer sequences used for reverse transcription and qPCR can be found in supplementary table 2.

To quantify the difference between the 3' and 5' located primer pairs, a modified version of the ddCq method was used where the 3' primer pair takes on the function of the housekeeping gene. First, to calculate the 3':5' dCq values, the 3' Cq value was subtracted from the 5' Cq value for each sample. Next, to calculate the 3':5' ddCq, the mean 3':5' dCq value of the empty transduction controls was subtracted from the 3':5' dCq values of the treatments.

Nanopore cDNA sequencing

The experiment and subsequent library preparation consisted of seven steps: (1) RNP transduction, (2) RNA isolation, (3) rRNA depletion, (4) poly(A) tailing, (5) reverse transcription, (6) second strand synthesis and (7) barcode and sequencing adapter ligation.

To ensure enough RNA for sequencing, this experiment was performed in 6-well plates, plating 600 000 HAP1-dEGFP^{Y66S} cells per well the day before the transductions. One well was reserved as a no transduction control. iTOP was performed as described above, using an iTOP mixture volume of 1 mL per well. Each timepoint had three conditions: an empty transduction control, a transduction with LbuCas13a and a non-targeting guide RNA, and a transduction with LbuCas13a and a dEGFP targeting guide RNA (SP2). Cells were collected in TRIzol at 0, 50, 100, 200, 400 and 1440 minutes after iTOP. Total RNA was isolated and DNase-treated as described above. RNA integrity was assessed on the Bioanalyzer. Next, 5 µg total RNA of each sample was used for rRNA depletion with the RiboMinus Eukaryotic system v2 (Invitrogen, A15026). rRNA depletion was confirmed with the Bioanalyzer. Then, the rRNA depleted RNA was poly(A)-tailed with *E. coli* Poly(A) polymerase (NEB, M0276L) in the presence of 1 mM ATP and 1 unit/uL RNasin® (Promega, N2515) for 30 minutes at 37ºC. Afterwards, the RNA was cleaned with the Zymo RNA Clean & Concentrator -5 Kit (R1013) according to the manufacturers instruction. Next, reverse transcription was performed using SuperScript IV RT (Invitrogen, 18090010) and anchored oligo dT_{20} primers (Supplementary table 2). The reverse transcription reaction was incubated at 50ºC for 15 minutes followed by 80ºC for 10 minutes. To remove RNA before second strand synthesis, 1 uL of RNase Cocktail (Thermo, AM2286) was added after reverse transcription and incubated at 37ºC for 20 minutes. For the second strand synthesis, 1 µL of 100 ng/µL random hexamer primers (Promega: C1181) was added to each

sample. Then, the NEBNext second strand synthesis kit (NEB, E6111) was used according to the manufacturer's instructions. dsDNA was purified using AMPure XP beads (Beckman Coulter: A63882) at a ratio of 2 beads to 1 sample. The NEBNext Ultra II End Repair/dA-tailing Module (NEB, E7546S) was used before ligating Nanopore native barcodes (EXP-NBD104&114). Finally, samples were pooled and the sequencing adapter (SQK-LSK109) was ligated. 1000 ng DNA was loaded on the Promethion flowcell (FLO-PRO002) and sequenced for 3 days. Two independent replicates of the entire nanopore sequencing experiment were performed.

Nanopore data analysis

During sequencing, the Nanopore MinKNOW software (version 21.11.7, Guppy version 5.1.13) called bases in real-time by the using the 'Super-accurate' base calling setting, demultiplexed samples and trimmed barcodes. For replicate 1, the 0 minute after transduction, dEGFP targeting sample had a very low DNA yield after library preparation and consequently much fewer reads than the other samples. Therefore, it was excluded from all analysis. Reads were mapped to the transcriptome using minimap2[57]. Transcriptome alignment was done using the *-ax map-ont* arguments, against a merge of the Ensemble Homo_sapiens.GRCh38.cdna.all (release 104), Ensemble Homo_sapiens.GRCh38.ncrna (release 104), the entire 51_EF-1a_dEGFP^{Y66S}-IRIS-PuroR-WPRE plasmid (Supplementary file 1) and the 18S and 28S ribosomal RNA. Only the primary alignment was used for analysis. To generate the density plots in Figure 3A and Supplementary figure 5B, all histone transcripts and WDR74 were excluded. Histone transcripts and WDR74 were so abundant that they obscured all other mRNAs in the density plot. The extremely high abundance of WDR74 was caused by a small nuclear RNA

mapping to WDR74-204. All analysis was performed in Rstudio, using data.table[68] and ShortRead[69] for data loading, Tidyverse[70] for data handling and ggplot2[71] for plotting. Raw sequencing reads are available online at https://www.ncbi.nlm.nih.gov/sra/PRJNA912090. The script used for calculating transcript coverages is available on https://github.com/JorikBot/cas13.

RNA sequencing and analysis

For the RNA-seq experiment, HAP1-dEGFP^{Y66S} cells were transfected using iTOP, as described above. The day before transfection, 600 000 cells per well had been plated in 6-well plates. Treatments were: an empty transfection, a transfection with LbuCas13a but no guide RNA, a transfection with LbuCas13a and a non-targeting guide RNA, and finally a transfection with LbuCas13a and a dEGFP targeting guide RNA (SP2). All treatments were done in triplicates. After 16 hours, cells were lysed in TRIzol reagent. Total RNA was isolated and DNase-treated as described above. mRNA was then extracted using a NEBNext Poly(A) mRNA Magnetic Isolation Module (NEB, E7490S) and RNA-seq libraries were prepared using a NEBNext Ultra Directional RNA Library Prep Kit for Illumina (NEB, E7420L). RNA-seq libraries were sequenced on an Illumina NextSeq500 Instrument with at least 10 million reads per library. An index was generated using the RefSeq GRCh37 assembly and reads were aligned and quantified using STAR[62] and featureCounts[63]. Differentially expressed genes were determined using DESeq2[72]. Genes with an adjusted P-value < 0.05 and log2(Fold Change) > |1| were regarded as differentially expressed genes, and they were subjected to subsequent enrichment analysis. GO term and pathway enrichment analysis was done using ShinyGO[73] V0.75, supplying all detected transcripts as background. RNA-seq data is available online at the NCBI

Gene expression omnibus (GSE220759). The code of the differential gene expression analysis is available on https://github.com/JorikBot/cas13.

Live cell imaging

The live cell imaging protocol used here was adapted from Wallberg *et al*.[58]. HAP1 and HAP1-dEGFP^{Y66S} cells were imaged in imaging medium (FluoroBrite™ DMEM, 10% FBS, 2.5 mM $CaCl_2$) supplemented with 2 µL CellTox™ Green (Promega, G8741) and 5 µL Annexin V-AV647 (Invitrogen, A23204) per milliliter. Cells were seeded in 8-well µ-Slides (ibidi, 80827) coated with a 1:100 dilution of Matrigel (Corning, 356231), plating 55 000 cells per well. The next day, iTOP was performed as described above, using an iTOP mixture volume of 200 µL per well. After removing the iTOP buffer, wells were washed with 300 µL PBS before adding 300 µL imaging medium. This extra PBS wash step prevents protein or salt precipitation during imaging. After iTOP, cells were allowed to recover in the cell culture incubator for up to four hours. Next, cells were moved to the Leica AF7000 and allowed to equilibrate for one hour (37°C, 5% CO_2). During live imaging, pictures were taken every 15 minutes at four positions per well for 20 hours, using a 20x Dry N.A. 0.50 objective. Finally, the amount of Annexin V and CellTox™ Green positive cells were counted with CellProfiler[74] using the IdentifyPrimaryObjects module.

Cell selection experiments

For the cell selection experiments, HAP1-EGFP cells were mixed with HAP1 cells at a ratio of roughly 4:1. HAP1-EGFP were selected against by introducing LbuCas13a with an EGPF

683 targeting guide RNA (SP2) using iTOP. The percentage of EGFP positive cells was measured
684 by FACS on the BD FACSCanto II (BD Bioscience). To generate HAP1-EGFP lines with
685 different levels of EGFP expression, cells were sorted into fifteen different populations with
686 increasing EGFP intensities using the BD FACSJazz cell sorter (BD Bioscience). We sorted the
687 cells in complete cell culture medium. After sorting, the three populations with the lowest EGFP
688 intensity were cultured in medium without puromycin. The next three lowest populations were
689 cultured at 2 µg/mL puromycin, the following groups of three at 5 µg/mL, 10 µg/mL and finally 20
690 µg/mL. For the selection experiment, the different EGFP lines were mixed with wildtype HAP1
691 cells and subjected to selection as described above. Additionally, in parallel they were also
692 plated in a separate well. These parallel wells were harvested in TRIzol immediately after the
693 mixed population had been subjected to iTOP, and used to determine their EGFP expression
694 levels. Conventional RT-qPCR was performed as described above for 3':5' RT-qPCR. qPCR
695 primers can be found in supplementary table 2.

696

697 To repair the dEGFP$^{\Delta fluor}$ mutation, cells were transduced with AsCas12a proteins, guide RNA
698 (Supplementary table 3) and a LAHR repair template (Supplementary table 3) using iTOP. For
699 each well of a 96-well plate, 50 µL of iTOP mixture that contained 20 µL of transduction
700 supplement B, 10 µL of AsCas12a protein (150 µM), 10 µL of guide RNA (300 µM) and 10 µL of
701 500 pmol repair template in nuclease-free water was used. Three days after iTOP transduction,
702 the cells that had not been edited were selected against by delivering LbuCas13a and a
703 dEGFP$^{\Delta fluor}$ targeting guide RNA (Supplementary table 1) using iTOP. Finally, the percentage of
704 EGFP positive cells was assessed on the BD FACSCanto II three days after selection with
705 LbuCas13a.

Acknowledgements

The novo Nordisk Foundation Center for Stem Cell Medicine (reNEW) is supported by a Novo Nordisk Foundation grant number NFF21CC0073729, as well a funding from NWO-TTW, the Princes Beatrix Muscle Foundation. Z.Z. was supported, in part, by the China Scolarship Councel. The authors thank Stefan van der Elst of the Hubrecht Institute FACS facility, The LUMC FACS facility and the Utrecht sequencing facility (USEQ) for technical help

Author contributions

JB experimental design, execution and help writing the manuscript, ZZ experimental design, execution and help writing the manuscript, DK technical assistance, PS experimental design experimental design and help writing the manuscript, NG conceptual and experimental design, project supervision and help writing the manuscript

Conflict of Interest

NG is co-founder of NTrans Technologies and Divvly. No conflicting interest

References

1. Oost J Van Der, Westra ER, Jackson RN, Wiedenheft B. Unravelling the structural and mechanistic basis of CRISPR – Cas systems. *Nat Rev Microbiol* 2014; **12**:479–492.
2. Mohanraju P, Makarova KS, Zetsche B, Zhang F, Koonin E V., Oost J van der. Diverse evolutionary roots and mechanistic variations of the CRISPR-Cas systems. *Science (80-)* 2016; **353**.
3. Marraffini LA. CRISPR-Cas immunity in prokaryotes. *Nature* 2015; **526**.

4. Makarova KS, Wolf YI, Iranzo J, *et al.* Evolutionary classification of CRISPR–Cas systems: a burst of class 2 and derived variants. *Nat Rev Microbiol* 2020; **18**:67–83.
5. Liu G, Lin Q, Jin S, Gao C. The CRISPR-Cas toolbox and gene editing technologies. *Mol Cell* 2022; **82**:333–347.
6. Sharma G, Sharma AR, Bhattacharya M, Lee SS, Chakraborty C. CRISPR-Cas9: A Preclinical and Clinical Perspective for the Treatment of Human Diseases. *Mol Ther* 2021; **29**:571–586.
7. Koonin E V., Makarova KS, Zhang F. Diversity, classification and evolution of CRISPR-Cas systems. *Curr Opin Microbiol* 2017; **37**:67–78.
8. Makarova KS, Wolf YI, Alkhnbashi OS, *et al.* An updated evolutionary classification of CRISPR–Cas systems. *Nat Rev Microbiol* 2015; **13**:722–736.
9. Abudayyeh OO, Gootenberg JS, Konermann S, *et al.* C2c2 is a single-component programmable RNA-guided RNA-targeting CRISPR effector. *Science (80-)* 2016; **353**.
10. Smargon AA, Cox DBT, Pyzocha NK, *et al.* Cas13b Is a Type VI-B CRISPR-Associated RNA-Guided RNase Differentially Regulated by Accessory Proteins Csx27 and Csx28. *Mol Cell* 2017; **65**:618–630.
11. Konermann S, Lotfy P, Brideau NJ, Oki J, Maxim N. Transcriptome engineering with RNA-targeting Type VI-D CRISPR effectors. *Cell* 2018:1–12.
12. Yan WX, Chong S, Zhang H, *et al.* Cas13d Is a Compact RNA-Targeting Type VI CRISPR Effector Positively Modulated by a WYL-Domain- Containing Accessory Protein. *Mol Cell* 2018:1–13.
13. Xu C, Zhou Y, Xiao Q, *et al.* Programmable RNA editing with compact CRISPR–Cas13 systems from uncultivated microbes. *Nat Methods* 2021; **18**:499–506.
14. Cox DBT, Gootenberg JS, Abudayyeh OO, *et al.* RNA editing with CRISPR-Cas13. *Science (80-)* 2017; **358**:1019–1027.
15. East-Seletsky A, O'Connell MR, Knight SC, *et al.* Two distinct RNase activities of CRISPR-C2c2 enable guide-RNA processing and RNA detection. *Nature* 2016; **538**:270–273.
16. Liu L, Li X, Wang J, *et al.* Two Distant Catalytic Sites Are Responsible for C2c2 RNase Activities. *Cell* 2017; **168**:121-134.e12.
17. Zhang C, Konermann S, Brideau NJ, *et al.* Structural Basis for the RNA-Guided Ribonuclease Activity of CRISPR-Cas13d Article Structural Basis for the RNA-Guided Ribonuclease Activity of CRISPR-Cas13d. *Cell* 2018; **175**:212-223.e17.
18. Slaymaker IM, Mesa P, Kellner MJ, *et al.* High-Resolution Structure of Cas13b and Biochemical Characterization of RNA Targeting and Cleavage. *Cell Rep* 2019; **26**:3741-3751.e5.
19. Knott GJ, East-Seletsky A, Cofsky JC, *et al.* Guide-bound structures of an RNA-targeting A-cleaving CRISPR–Cas13a enzyme. *Nat Struct Mol Biol* 2017.
20. Liu L, Li X, Ma J, *et al.* The Molecular Architecture for RNA-Guided RNA Cleavage by Cas13a. *Cell* 2017; **170**:714-726.e10.
21. East-Seletsky A, O'Connell MR, Burstein D, Knott GJ, Doudna JA. RNA Targeting by Functionally Orthogonal Type VI-A CRISPR-Cas Enzymes. *Mol Cell* 2017; **66**:373–383.
22. Meeske AJ, Nakandakari-Higa S, Marraffini LA. Cas13-induced cellular dormancy prevents the rise of CRISPR-resistant bacteriophage. *Nature* 2019.
23. East-Seletsky A, O'Connell MR, Burstein D, *et al.* RNA Targeting by Functionally Orthogonal Type VI-A CRISPR-Cas Enzymes. *Mol Cell* 2017; **66**:373-383.e3.
24. Gootenberg JS, Abudayyeh OO, Lee JW, *et al.* Nucleic acid detection with CRISPR-

Cas13a/C2c2. *Science (80-)* 2017; **356**:438–442.
25. Gootenberg JS, Abudayyeh OO, Kellner MJ, Joung J, Collins JJ, Zhang F. Multiplexed and portable nucleic acid detection platform with Cas13, Cas12a, and Csm6. *Science (80-)* 2018; **444**.
26. Myhrvold C, Freije CA, Gootenberg JS, *et al.* Field-deployable viral diagnostics using CRISPR-Cas13. *Science (80-)* 2018; **448**:444–448.
27. Fozouni P, Son S, Derby MD de L, *et al.* Amplification-free detection of SARS-CoV-2 with CRISPR-Cas13a and mobile phone microscopy. *Cell* 2021; **184**:323–333.
28. Arizti-sanz J, Freije CA, Stanton AC, *et al.* Integrated sample inactivation, amplification, and Cas13-based detection of SARS-CoV-2 Jon. *bioRxiv* 2020.
29. Patchsung M, Jantarug K, Pattama A, *et al.* Clinical validation of a Cas13-based assay for the detection of SARS-CoV-2 RNA. *Nat Biomed Eng* 2020; **4**.
30. Mohanraju P, Saha C, van Baarlen P, Louwen R, Staals RHJ, van der Oost J. Alternative functions of CRISPR–Cas systems in the evolutionary arms race. *Nat Rev Microbiol* 2022; **0123456789**.
31. Abudayyeh OO, Gootenberg JS, Essletzbichler P, *et al.* RNA targeting with CRISPR–Cas13. *Nature* 2017.
32. He B, Peng W, Huang J, *et al.* Modulation of metabolic functions through Cas13d-mediated gene knockdown in liver. *Protein Cell* 2020; **11**:518–524.
33. Zhang Y, Nguyen TM, Zhang XO, *et al.* Optimized RNA-targeting CRISPR/Cas13d technology outperforms shRNA in identifying functional circRNAs. *Genome Biol* 2021; **22**:1–22.
34. Li S, Li X, Xue W, *et al.* Screening for functional circular RNAs using the CRISPR–Cas13 system. *Nat Methods* 2021; **18**:51–59.
35. Huynh N, Depner N, Larson R, King-Jones K. A versatile toolkit for CRISPR-Cas13-based RNA manipulation in Drosophila. *Genome Biol* 2020; **21**:1–29.
36. Kushawah G, Hernandez-Huertas L, Abugattas-Nuñez del Prado J, *et al.* CRISPR-Cas13d Induces Efficient mRNA Knockdown in Animal Embryos. *Dev Cell* 2020; **54**:805-817.e7.
37. Zhou H, Su J, Hu X, *et al.* Glia-to-Neuron Conversion by CRISPR-CasRx Alleviates Symptoms of Neurological Disease in Mice. *Cell* 2020; **181**:590–603.
38. Powell JE, Lim CKW, Krishnan R, *et al.* Targeted gene silencing in the nervous system with CRISPR-Cas13. *Sci Adv* 2022; **8**.
39. Wang Q, Liu Y, Han C, *et al.* Efficient RNA Virus Targeting via CRISPR/CasRx in Fish. *J Virol* 2021; **95**.
40. Jing X, Xie B, Chen L, *et al.* Implementation of the CRISPR-Cas13a system in fission yeast and its repurposing for precise RNA editing. *Nucleic Acids Res* 2018; **46**:e90.
41. Mahas A, Aman R, Mahfouz M. CRISPR-Cas13d mediates robust RNA virus interference in plants. *Genome Biol* 2019:1–16.
42. Aman R, Ali Z, Butt H, *et al.* RNA virus interference via CRISPR/Cas13a system in plants. *Genome Biol* 2018; **19**:1.
43. Freije CA, Myhrvold C, Boehm CK, *et al.* Programmable Inhibition and Detection of RNA Viruses Using Cas13. *Mol Cell* 2019:1–12.
44. Tng PYL, Carabajal Paladino L, Verkuijl SAN, *et al.* Cas13b-dependent and Cas13b-independent RNA knockdown of viral sequences in mosquito cells following guide RNA expression. *Commun Biol* 2020; **3**.
45. Blanchard EL, Vanover D, Bawage SS, *et al.* Treatment of influenza and SARS-CoV-2 infections via mRNA-encoded Cas13a in rodents. *Nat Biotechnol* 2021; **39**:717–726.

46. Wang Q, Liu X, Zhou J, *et al.* The CRISPR-Cas13a Gene-Editing System Induces Collateral Cleavage of RNA in Glioma Cells. *Adv Sci* 2019; **1901299**.
47. Zhang Z, Wang Q, Liu Q, Zheng Y, Zheng C, Yi K. Dual-Locking Nanoparticles Disrupt the PD-1 / PD-L1 Pathway for Efficient Cancer Immunotherapy. *Adv Mater* 2019; **1905751**:1–10.
48. Özcan A, Krajeski R, Ioannidi E, *et al.* Programmable RNA targeting with the single-protein CRISPR effector Cas7-11. *Nature* 2021; **597**.
49. Buchman AB, Brogan DJ, Sun R, Yang T, Hsu PD, Akbari OS. Programmable RNA Targeting Using CasRx in Flies. *Cris J* 2020; **3**:164–176.
50. Li Y, Xu J, Guo X, *et al.* Collateral cleavage of 28s rRNA by RfxCas13d causes death of mice. *bioRxiv* 2022.
51. Shi P, Murphy MR, Aparicio AO, *et al.* RNA-guided cell targeting with CRISPR/RfxCas13d collateral activity in human cells. *bioRxiv* 2021.
52. Ai Y, Liang D, Wilusz JE. CRISPR/Cas13 effectors have differing extents of off-target effects that limit their utility in eukaryotic cells. *Nucleic Acids Res* 2022; **50**:1–16.
53. D'Astolfo DS, Pagliero RJ, Pras A, *et al.* Efficient intracellular delivery of native proteins. *Cell* 2015; **161**:674–690.
54. Zhao Z, Shang P, Sage F, Geijsen N. Ligation-assisted homologous recombination enables precise genome editing by deploying both MMEJ and HDR. *Nucleic Acids Res* 2022; **50**:e62–e62.
55. Bot JF, van der Oost J, Geijsen N. The double life of CRISPR–Cas13. *Curr Opin Biotechnol* 2022; **78**:102789.
56. Nolan T, Hands RE, Bustin SA. Quantification of mRNA using real-time RT-PCR. *Nat Protoc* 2006; **1**:1559–1582.
57. Li H. Minimap2: Pairwise alignment for nucleotide sequences. *Bioinformatics* 2018; **34**:3094–3100.
58. Wallberg F, Tenev T, Meier P. Time-lapse imaging of cell death. *Cold Spring Harb Protoc* 2016; **2016**:251–258.
59. Olmo N, Turnay J, De Buitrago GG, De Silanes IL, Gavilanes JG, Lizarbe MA. Cytotoxic mechanism of the ribotoxin α-sarcin: Induction of cell death via apoptosis. *Eur J Biochem* 2001; **268**:2113–2123.
60. Andrews S. FastQC: A Quality Control Tool for High Throughput Sequence Data [Online]. 2010.
61. Wang L, Wang S, Li W. RSeQC: Quality control of RNA-seq experiments. *Bioinformatics* 2012; **28**:2184–2185.
62. Dobin A, Davis CA, Schlesinger F, *et al.* STAR: Ultrafast universal RNA-seq aligner. *Bioinformatics* 2013; **29**:15–21.
63. Liao Y, Smyth GK, Shi W. FeatureCounts: An efficient general purpose program for assigning sequence reads to genomic features. *Bioinformatics* 2014; **30**:923–930.
64. Tong H, Huang J, Xiao Q, *et al.* High-fidelity Cas13 variants for targeted RNA degradation with minimal collateral effect. *bioRxiv* 2021:2021.12.18.473271.
65. Tong H, Huang J, Xiao Q, *et al.* High-fidelity Cas13 variants for targeted RNA degradation with minimal collateral effects. *Nat Biotechnol* 2022.
66. Vialetto E, Yu Y, Collins SP, Wandera KG, Barquist L, Beisel CL. A target expression threshold dictates invader defense and prevents autoimmunity by CRISPR-Cas13. *Cell Host Microbe* 2022:1–12.
67. Signorell A et mult. al. DescTools: Tools for descriptive statistics. 2021.

68. Dowle M, Srinivasan A. data.table: Extension of “data.frame.” 2022.
69. Morgan M, Anders S, Lawrence M, Aboyoun P, Pagès H, Gentleman R. ShortRead: A bioconductor package for input, quality assessment and exploration of high-throughput sequence data. *Bioinformatics* 2009; **25**:2607–2608.
70. Wickham H, Averick M, Bryan J, *et al.* Welcome to the Tidyverse. *J Open Source Softw* 2019; **4**:1686.
71. Wickham H. A Layered grammar of graphics. *J Comput Graph Stat* 2010; **19**:3–28.
72. Love MI, Huber W, Anders S. Moderated estimation of fold change and dispersion for RNA-seq data with DESeq2. *Genome Biol* 2014; **15**.
73. Ge SX, Jung D, Jung D, Yao R. ShinyGO: A graphical gene-set enrichment tool for animals and plants. *Bioinformatics* 2020; **36**:2628–2629.
74. McQuin C, Goodman A, Chernyshev V, *et al.* CellProfiler 3.0: Next-generation image processing for biology. *PLoS Biol* 2018; **16**:1–17.
75. Zuker M. Mfold web server for nucleic acid folding and hybridization prediction. *Nucleic Acids Res* 2003; **31**:3406–3415.
76. Consortium Rna. RNAcentral 2021: Secondary structure integration, improved sequence search and new member databases. *Nucleic Acids Res* 2021; **49**:D212–D220.
77. Crooks G, Hon G, Chandonia J, Brenner S. WebLogo: A Sequence Logo Generator. *Genome Res* 2004; **14**:1188–1190.
78. Blighe K, Rana S, Lewis M. EnhancedVolcano: Publication-ready volcano plots with enhanced colouring and labeling. 2022.

Figure legends

Figure 1. LbuCas13a has collateral cleavage activity in human cells. A RNaseAlert assay. The rate was calculated by taking the slope of the initial linear increase in fluorescence intensity. **B** Schematic depiction of the 3’:5’ qPCR assay. Arrows indicate the 5’ and 3’ primer pairs used for qPCR. **C** Cleavage of target (dEGFP) and collateral (GAPDH) RNA as assessed by the 3’:5’ qPCR assay (n=3). P-values calculated by Welch t-test (ns = not significant, * < 0.05, ** < 0.01). Small dots are independent replicates. Big dot and line show mean and standard error of the mean. **D** Total RNA profiles at various timepoints after transduction (n=3). Both HAP1 and HAP1-dEGFP cells were transduced with LbuCas13a and a dEGFP targeting guide RNA. The bottom zoomed in panels are corrected for differences in amount of loaded RNA. **E** 3’:5’ qPCR assay (n=3) on samples from **D**. Line shows ggplot2’s default LOESS regression. Since HAP1 cells do not contain dEGFP, no qPCR on dEGFP was performed for these cells.

Supplementary figure 1. Protein production and RNA yield after dEGFP targeting. *A* SDS-PAGE gel of Cas13 orthologs after HIS-tag purification followed by fast protein liquid chromatography (FPLC) gel filtration. **B** Concentration of isolated RNA decreases after dEGFP targeting in dEGFP expressing cells (n=3).

Figure 2. LbuCas13a is capable of collateral cleavage in different cell lines and targeting endogenous genes. *A, C, E* Total RNA profiles after 18S rRNA, GAPDH and RPS19 targeting respectively. RNA isolated 100 minutes after transduction. Bioanalyzer fluorescence values were normalized to the total area under the curve of each sample. n=3, except for the U2OS 18S rRNA, U2OS GAPDH and ARPE19 non-targeting samples, where n=2. **B, D, F** Quantification of rRNA cleavage in different cell lines, by taking the area under the curve of the region outlined by the grey boxes in **A, C, E**. **G** 3':5' RT-qPCR assays on samples from **A, C, E** (n=3). Dot and line show mean and standard error of the mean.

Supplementary figure 2. Collateral RNA cleavage after delivery by electroporation. A Total RNA profiles at 200 and 400 minutes after electroporation with LbuCas13a and a GAPDH, RPS19, 18S rRNA or non-targeting guide RNA. **B** Total RNA profiles 200 minutes after electroporation of HAP1 and HEK293T cells. For both **A** and **B**: fluorescence intensity was adjusted to the total area under the curve of each sample, and n=3.

Supplementary figure 3. Cas13 Orthologs. A-C Total RNA profiles after GAPDH, dEGFP and 18S rRNA targeting with (**A**) LwaCas13a, (**B**) BzCas13b and (**C**) RspCas13d. RNA isolated 100 minutes after transduction using iTOP. Fluorescence was adjusted to the total area under the curve, to equalize for differences in loaded amount of RNA. n=3.

Figure 3. Nanopore sequencing after collateral cleavage by LbuCas13a. A Density plot of read length versus reference transcript length of all reads mapped to protein coding transcripts, excluding histone genes and WDR74. Columns show minutes post transduction. Data from replicate 2, see Supplementary figure 5A for replicate 1. **B, C** Transcript coverage of (**B**) the target transcript dEGFP-IRIS-PuroR and (**C**) RPS19-202. Columns show minutes post transduction. The 0 minutes post transduction, dEGFP targeting sample of replicate 1 was excluded due to failed library preparation. For **B**, reads were aligned to the entire plasmid sequence used to make this cell line. The start and stop codon are at position 3415 and 5316 respectively. The dotted lines indicate the protospacer position.

Supplementary figure 4. Nanopore library preparation and read length. A Total RNA profiles of the samples send for Nanopore sequencing. **B** Bioanalyzer RNA profile after rRNA depletion. Legends same as **A. C** Rolling mean (k = 20) of the read lengths, corrected by the total amount of reads in each sample. The spike at ~4000 nt in the 50 minute replicate 1 sample is probably rRNA contamination, see **B**. Legends same as **A.**

Supplementary figure 5. Protein coding transcripts are affected by collateral cleavage. A Density plot of read length versus reference transcript length of all reads mapped to protein coding transcripts, excluding histone genes and WDR74 (see M&M). Data from replicate 1. **B** Percentage of all reads that mapped to various transcript biotypes. rRNA mapped reads were excluded due to variability in rRNA depletion efficiencies.

Figure 4. LbuCas13a collateral RNA cleavage sites in human cells. A Transcript coverage of non-target RNAs, zoomed in at putative cleavage sites. **B** The predicted RNA structures at the putative cleavage sites from **A**. Red letters are the approximate location of the coverage dips, corresponding to the dashed lines in **A**. RNA structures for RPS19-202 and GAPDH-205 are the top predictions of Mfold[75] using the default setting. 18S rRNA structure provided by RNAcentral.org[76] (URS0000726FAB_9606). **C** Sequence logo around 100 manually annotated cleavage sites. The U at position 0 was enforced during potential cleavage site selection. Logo made using WebLogo[77].

Supplementary figure 6. mRNAs are cleaved at specific positions by LbuCas13a. **A-C** Transcript coverage of (**A**) PKM-202, (**B**) GAPDH-205 and (**C**) ACTB-217. Columns show minutes post transduction.

Supplementary figure 7. Cytoplasmic ncRNA are cleaved by LbuCas13a. A-C Transcript coverage of (**A**) RN7SL1-201, (**B**) 18S rRNA and (**C**) 28S rRNA. Columns show minutes post transduction.

Supplementary figure 8. Transcript coverage of some nuclear and a mitochondrial RNA. A-C Transcript coverage of (**A**) U1, (**B**) RN7SK and (**C**) MT-RNR1. Columns show minutes post transduction.

Figure 5. Cellular response after collateral RNA cleavage by LbuCas13a. A Pictures taken 24 hours after transduction. Scale bar is 50 µM. **B** Total amount of positive cells during live imaging after transduction. CTRL is an empty transduction. SP1, SP2 and SP3 are transductions with LbuCas13a and three different guide RNAs all targeting dEGFP. Quantified using CellProfiler[74]. **C** RNA-Seq EnhancedVolcano[78] plot of dEGFP targeting samples vs controls, n=3. Dotted lines indicate P-value = 0.05 and |Log2 FC| = 1. **D** Top enriched GO biological processes using the significantly upregulated genes (adjusted P value < 0.05 & Log2 FC > 1). Plot generated using ShinyGo[73].

Supplementary figure 9. RNA-seq data analysis. A Ratio between the percentage of reads mapped to exons and introns. **B** PCA plot of the RNA-seq samples using the default setting of the plotPCA function in DESeq2[72]. **C** Top enriched GO molecular functions using the

significantly upregulated genes. Plot generated using ShinyGo[73]. **D** KEGG pathway enrichment of the significantly upregulated genes. Plot generated using ShinyGo[73].

Figure 6. LbuCas13a as a cell selection tool. A Schematic of the Cas13-based cell selection. **B** Depletion of EGFP positive cells after EGFP targeting. Trendlines show a generalized additive model using formula y ~ s(x, k = 6). **C** Multiple targeting rounds improve EGFP depletion. Error bars show standard deviation. **D** Schematic showing creation of cell lines with different EGFP expression levels and subsequent selection experiments. **E** Target expression level determines depletion efficiency. Trendlines created by LOESS regression. **F** Enrichment of edited cells by targeting them with LbuCas13a. Error bars show standard deviation. P-values calculated by Welch's t-test (ns = not significant, **** = P-value < 0.0001).

Supplementary figure 10. Generating lines with various levels of EGFP expression and gene editing strategy. A Gating strategy to sort different EGFP intensities. **B** A wide range of EGFP expression levels were recovered after sorting. **C** Schematic showing the LAHR editing strategy, see Zhao et al. for details[54].

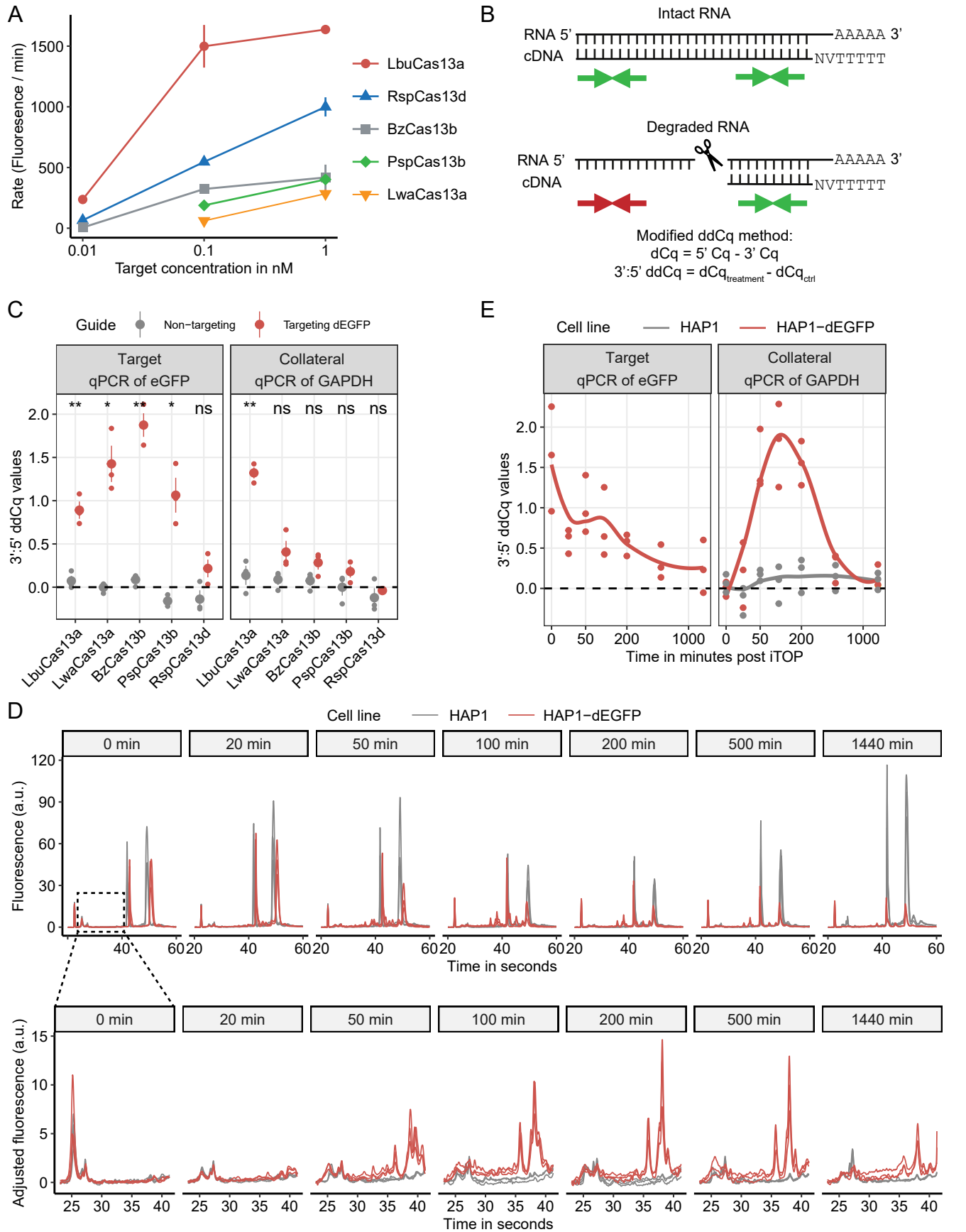

J. F. Bot et al. Figure 1

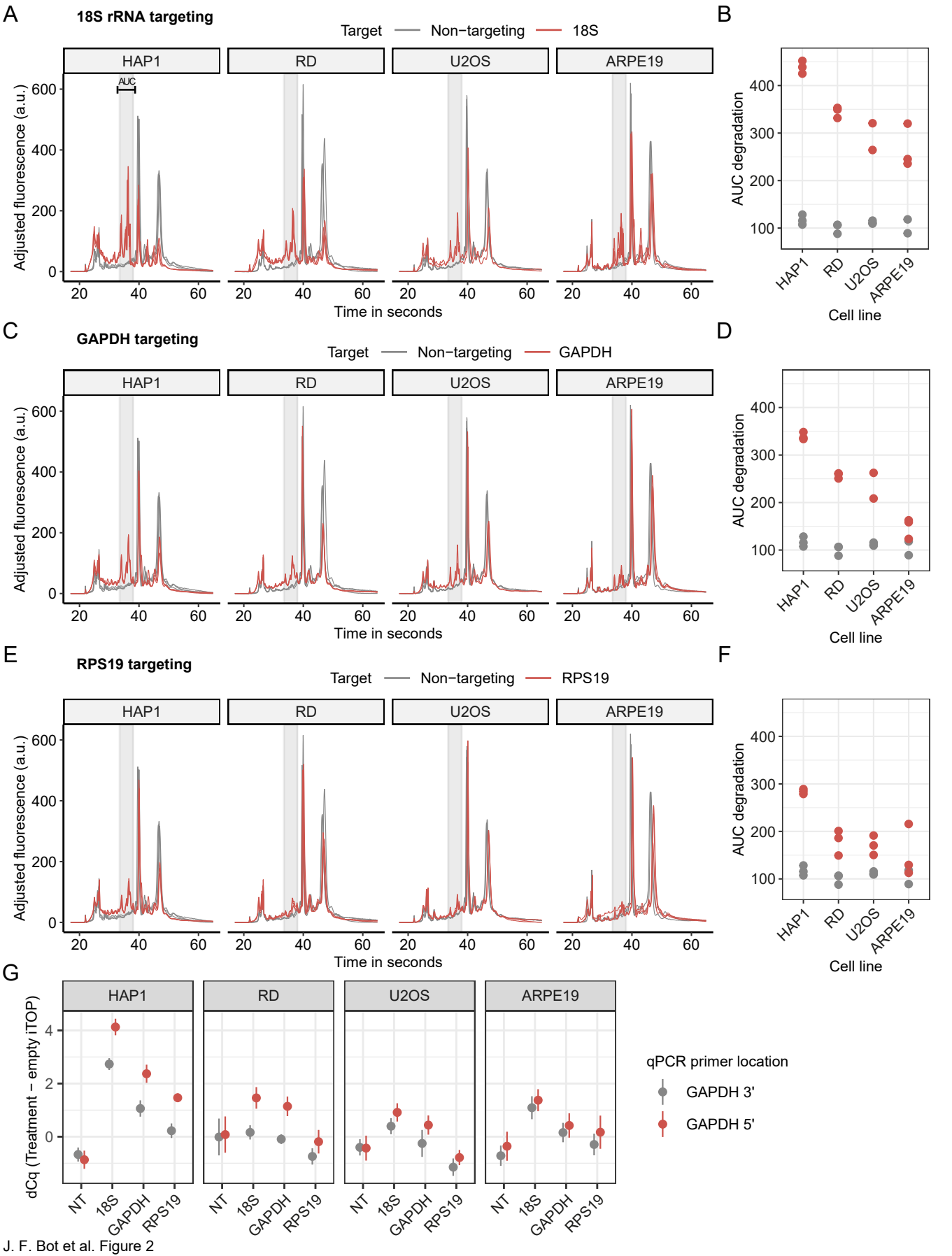

J. F. Bot et al. Figure 2

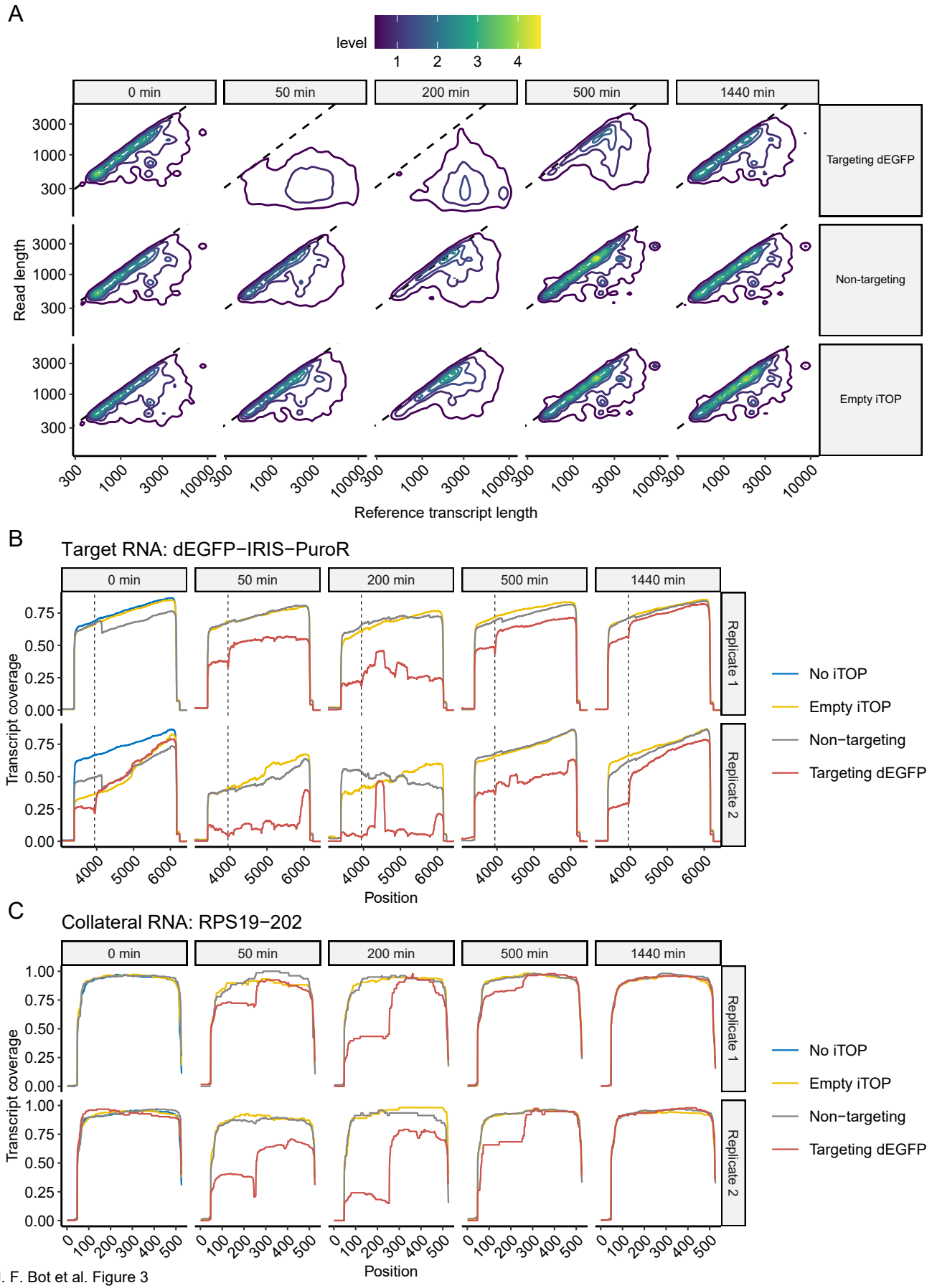

J. F. Bot et al. Figure 3

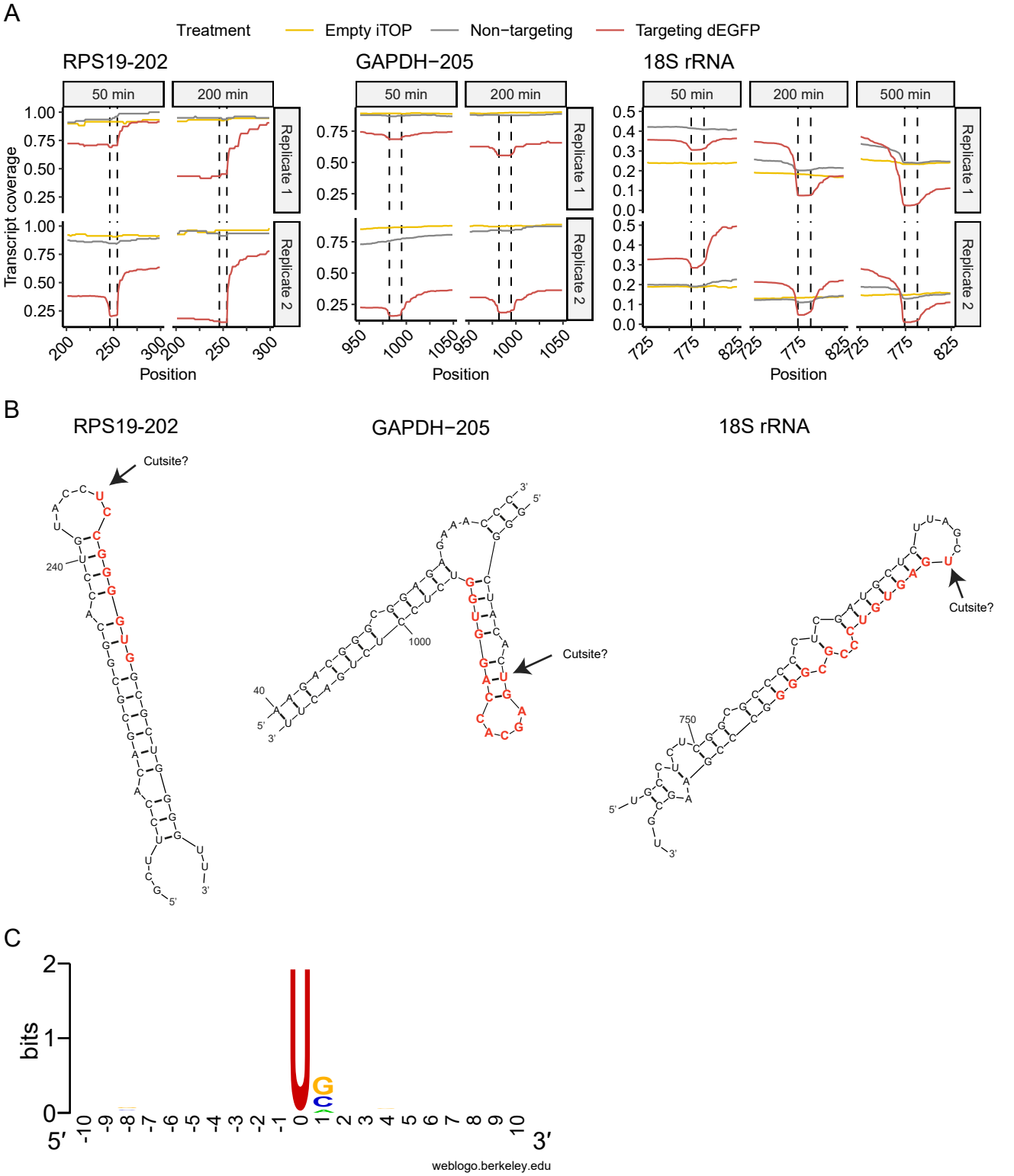

J. F. Bot et al. Figure 4

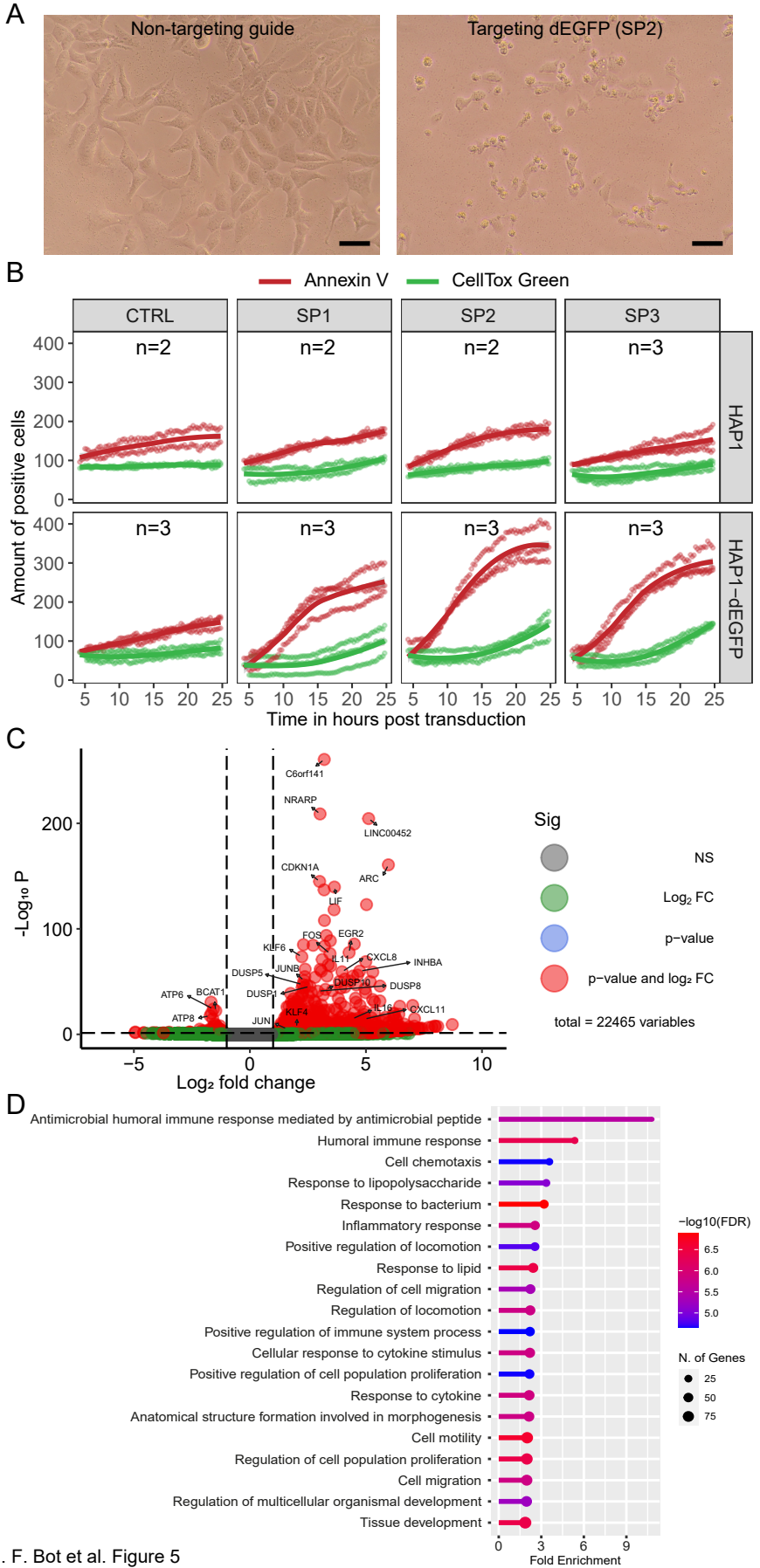

J. F. Bot et al. Figure 5

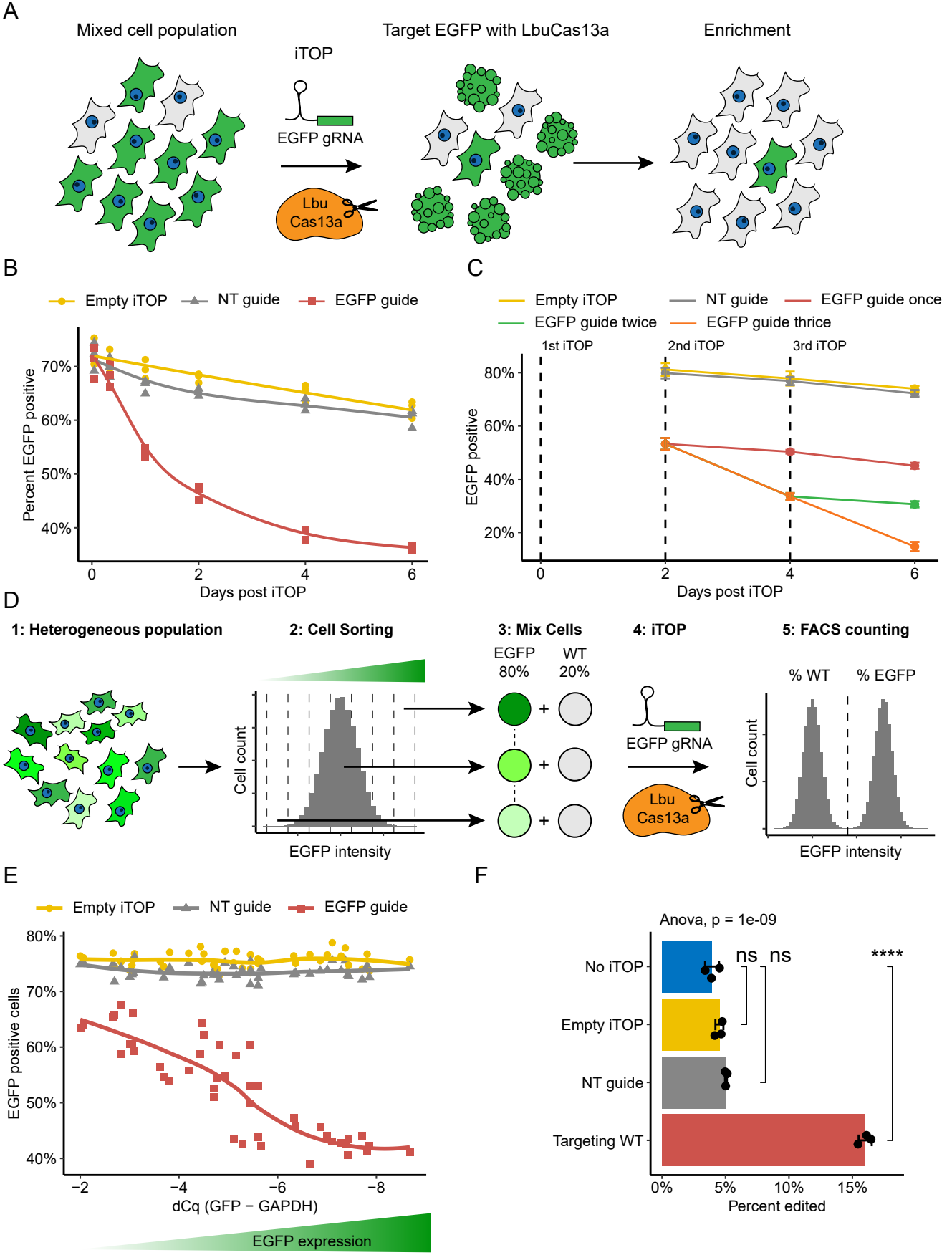

J. F. Bot et al. Figure 6